Developmental Cognitive Neuroscience 12 (2015) 123–133

Contents lists available at ScienceDirect

Developmental Cognitive Neuroscience

journal homepage: http://www.elsevier.com/locate/dcn

Accurate age classification of 6 and 12 month-old infants based on resting-state functional connectivity magnetic resonance imaging data

John R. Pruett Jr.[a,*], Sridhar Kandala[a], Sarah Hoertel[a], Abraham Z. Snyder[a], Jed T. Elison[b], Tomoyuki Nishino[a], Eric Feczko[c], Nico U.F. Dosenbach[a], Binyam Nardos[a], Jonathan D. Power[d], Babatunde Adeyemo[a], Kelly N. Botteron[a], Robert C. McKinstry[a], Alan C. Evans[e], Heather C. Hazlett[f], Stephen R. Dager[g], Sarah Paterson[h], Robert T. Schultz[h], D. Louis Collins[e], Vladimir S. Fonov[e], Martin Styner[f], Guido Gerig[i], Samir Das[e], Penelope Kostopoulos[e], John N. Constantino[a], Annette M. Estes[g], The IBIS Network[1], Steven E. Petersen[a], Bradley L. Schlaggar[a], Joseph Piven[f]

[a] *Washington University School of Medicine in St. Louis, 660 South Euclid Avenue, St. Louis, MO 63110, United States*
[b] *University of Minnesota, 51 East River Parkway, Minneapolis, MN 55455, United States*
[c] *Emory University, 201 Dowman Drive, Atlanta, GA 30322, United States*
[d] *National Institute of Mental Health, National Institutes of Health, 10 Center Drive, Bethesda, MD 20814, United States*
[e] *McConnell Brain Imaging Center, Montreal Neurological Institute, McGill University, 3801 University Street, Montreal, QC, Canada H3A 2B4*
[f] *University of North Carolina at Chapel Hill, 101 Manning Drive, Chapel Hill, NC 27514, United States*
[g] *University of Washington, Seattle, 1410 NE Campus Parkway, Seattle, WA 98195, United States*
[h] *Children's Hospital of Philadelphia and University of Pennsylvania, Civic Center Boulevard, Philadelphia, PA 19104, United States*
[i] *University of Utah, Salt Lake City, 201 Presidents Circle, Salt Lake City, UT 84112, United States*

ARTICLE INFO

Article history:
Received 15 August 2014
Received in revised form 14 January 2015
Accepted 16 January 2015
Available online 3 February 2015

Keywords:
Functional connectivity magnetic resonance imaging (fcMRI)

ABSTRACT

Human large-scale functional brain networks are hypothesized to undergo significant changes over development. Little is known about these functional architectural changes, particularly during the second half of the first year of life. We used multivariate pattern classification of resting-state functional connectivity magnetic resonance imaging (fcMRI) data obtained in an on-going, multi-site, longitudinal study of brain and behavioral development to explore whether fcMRI data contained information sufficient to classify infant age. Analyses carefully account for the effects of fcMRI motion artifact. Support vector machines (SVMs) classified 6 versus 12 month-old infants (128 datasets) above chance based on fcMRI

* Corresponding author at: Washington University School of Medicine, 660 South Euclid Avenue, Campus Box 8134, St. Louis, MO 63110, United States. Tel.: +1 314 747 6792; fax: +1 314 747 6777.
E-mail addresses: pruettj@psychiatry.wustl.edu (J.R. Pruett Jr.), kandalas@psychiatry.wustl.edu (S. Kandala), sarah.hoertel@gmail.com (S. Hoertel), avi@npg.wustl.edu (A.Z. Snyder), jtelison@umn.edu (J.T. Elison), nishinot@mir.wustl.edu (T. Nishino), eric.j.feczko@emory.edu (E. Feczko), nico@npg.wustl.edu (N.U.F. Dosenbach), binyamn@npg.wustl.edu (B. Nardos), jonathan.power@nih.gov (J.D. Power), adeyemob@cabernet.wustl.edu (B. Adeyemo), botteronk@mir.wustl.edu (K.N. Botteron), mckinstryb@mir.wustl.edu (R.C. McKinstry), alan.acehigh@gmail.com (A.C. Evans), Heather_Cody@med.unc.edu (H.C. Hazlett), srd@u.washington.edu (S.R. Dager), patersons@email.chop.edu (S. Paterson), schultzrt@email.chop.edu (R.T. Schultz), louis.collins@mcgill.ca (D.L. Collins), vladimir.fonov@mcgill.ca (V.S. Fonov), styner@cs.unc.edu (M. Styner), gerig@sci.utah.edu (G. Gerig), samir@bic.mni.mcgill.ca (S. Das), penelope.kostopoulos@mcgill.ca (P. Kostopoulos), constanj@psychiatry.wustl.edu (J.N. Constantino), estesa@u.washington.edu (A.M. Estes), sep@npg.wustl.edu (S.E. Petersen), schlaggarb@neuro.wustl.edu (B.L. Schlaggar), joe_piven@med.unc.edu (J. Piven).
[1] See Appendix A for members of IBIS Network.

http://dx.doi.org/10.1016/j.dcn.2015.01.003

Infant
Development
Multivariate pattern analysis (MVPA)
Support vector machine (SVM)
Functional brain networks

data alone. Results demonstrate significant changes in measures of brain functional organization that coincide with a special period of dramatic change in infant motor, cognitive, and social development. Explorations of the most different correlations used for SVM lead to two different interpretations about functional connections that support 6 versus 12-month age categorization.

1. Introduction

The 6–12 month period in infant development has not been well characterized by fcMRI. Here, we asked whether fcMRI data from 6 and 12 month-old infants contain sufficient information to support age classification after rigorous motion artifact rejection. Many sophisticated cognitive and social capacities begin to consolidate during the latter half of the first year of human life, which is characterized by the emergence of joint attention (Scaife and Bruner, 1975), specialization of face identity discrimination (Pascalis et al., 2002) and phoneme specification (Kuhl et al., 2003), the emergence of perceptual binding (Csibra et al., 2000), and perhaps the emergence of perceptual consciousness (Kouider et al., 2013). Additionally, increasing motor control and mobility (e.g., active crawling and walking, assisted and unassisted) alter the perspective by which an infant explores and accesses the world during this period. The magnitude and multifaceted nature of typical developmental changes across 6–12 months, therefore, lead us to predict significant and widespread differences in brain functional connectivity across these ages.

Typical and atypical developmental processes are hypothesized to relate to the developmental reorganization of large-scale functional brain networks that support various sensory, motor, and cognitive functions (Johnson, 2001). Functional connectivity magnetic resonance imaging (fcMRI) has shown great promise for characterizing these networks (Power et al., 2011; Yeo et al., 2011). Prior infant fcMRI studies (reviewed in Hoff et al. (2013)) have primarily covered the 0–24 month time period. These studies have demonstrated the presence of resting state functional connectivity networks at birth during natural sleep (Fransson et al., 2009); effects of prematurity (Doria et al., 2010; Smyser et al., 2010); and functional architectural changes from two weeks to one year to two years (Lin et al., 2008), with a focus on the default mode network (Gao et al., 2009). Investigators have studied changing functional network properties from three weeks to one year to two years, including small world and efficiency metrics and the characterizations of network hubs (Gao et al., 2011; see Fransson et al. (2011) for analyses of "hubs" at birth) and the development of interactions between different networks (Gao et al., 2013). Some investigators have reported increasing long- /decreasing short-range functional connectivity, with increased default mode network connectivity between four and nine months (Damaraju et al., 2013).

The 6–12-month period is important for typical development and, we believe, for the development of autism spectrum disorder (ASD), and investigators have only recently begun to characterize it in detail using fcMRI (Gao et al., 2014). During this time, gaze following and social referencing consolidate; imitative learning emerges; infants initiate the use of communicative gestures; and social interactions shift from dyadic to triadic (person–person–object). The 6–12-month period, referred to as a "social-cognitive revolution" (Tomasello, 2000, p. 38), sets the stage for a host of increasingly sophisticated social behaviors. It is, therefore, important to learn more about which brain functional connections allow for classification of age across this developmental period. Prior results in older subjects supporting hypotheses of developmental change in large-scale functional brain networks have recently been called into question because of increasing appreciation of the age-mimicking, artifactual effects that sub-millimeter movements create in fcMRI data from older subjects (Power et al., 2012, 2014; Satterthwaite et al., 2013; Van Dijk et al., 2012). In this report we use "state of the art" frame-censoring motion artifact rejection procedures (Power et al., 2014).

We examined fcMRI network changes between 6 and 12 months of age in 92 infants of whom 36 infants had both 6 and 12 month scans (128 total datasets). The current fMRI data preprocessing strategy incorporates several recent advances that minimize the impact of head motion artifact more effectively than in prior studies. We employ support vector machine (SVM) (Ben-Hur et al., 2008) multivariate pattern classification to (1) exploit the information content of fcMRI data, which intrinsically is of high dimension, (2) explore which connections contribute to significant classifications, and (3) lay the foundation for developing predictive classifiers to aid early risk assessment in ASD. fcMRI data acquired from naturally sleeping infants were processed according to recent analytic and motion cleaning recommendations (Power et al., 2014), with infant-specific adaptations to initial registration and nuisance regression steps. fcMRI matrices were constructed using 230 functionally defined seed regions (culled from 264 in Power et al. (2011) plus 16 additionally derived from Philip et al. (2012)) that were appropriately positioned in gray matter at both ages. Support vector machine (SVM) methods involved recent adaptations of those used by some of the authors (Dosenbach et al., 2010).

2. Methods

The high- and low-risk infant groups, defined below (Section 2.1), provided independent samples within which to test SVM classification of infant age. Secondary analyses explored classification of risk (not diagnosis) at each age. These results were not significant; therefore, we combined risk groups for further tests of age classification.

Table 1
Subject age.

Age group	High risk mean age	High risk age SD	Low risk mean age	Low risk age SD	*df*	*t*	*p*
6 months	6.60	0.720	6.36	0.480	62	1.03	0.307
12 months	12.6	0.360	12.5	0.360	62	1.14	0.258
All	9.58	3.08	9.45	3.09	126	0.237	0.813

2.1. Inclusion criteria

A high-familial-risk-for-ASD and low-familial-risk-for-ASD cohort of infants was recruited for this study as part of a National Institutes of Health-funded, multi-site, Autism Centers of Excellence (ACE) Network study: the Infant Brain Imaging Study (IBIS). Subjects were excluded for comorbid medical or neurological diagnoses influencing growth, development, or cognition; prior genetic conditions; premature birth or low birth weight; maternal substance abuse during pregnancy; contraindication for MRI; or familial history of psychosis, schizophrenia, or bipolar disorder (Elison et al., 2013b; Wolff et al., 2012). High-risk infants were defined as having at least one sibling with an ASD diagnosis. Low-risk infants had at least one typically developing older sibling and did not have any first or second degree family members with ASD or intellectual disability. 6-Month-old infants were included if their age at scan acquisition was between 5.5 and 8.6 months (mean ± SD = 6.5 ± 0.6). 12-Month-old infants were included if their scan age was between 11.0 and 13.8 months (12.5 ± 0.4).

All subjects included in these analyses participated in a comprehensive battery of behavioral assessments and received an Autism Diagnostic Observation Schedule (ADOS: Lord et al., 2000) at 24 months of age. ADOSs and all other testing and interview data were independently reviewed by expert clinicians for DSM-IV-TR (American Psychiatric Association, 2000) criteria for autistic disorder or pervasive developmental disorder not otherwise specified. This paper focuses on data from infants who, at 24 months of age, did *not* meet criteria for ASD according to the ADOS (Gotham et al., 2007) and clinical best estimate using DSM-IV-TR criteria.[2]

2.2. Demographics

Four cohorts were defined: 6-month low-risk, 12-month low-risk, 6-month high-risk, and 12-month high-risk ($n = 32$ datasets per group; $n = 128$ total datasets from 92 unique infants, 36 of whom were scanned at both ages). These groups of 32 were pseudorandomly selected from $n = 164$ total (6- and 12-month ASD-negative subject) datasets that met our fcMRI quality control criteria and IBIS Network behavioral and structural MRI inclusion criteria. This procedure ensured balanced SVM runs, as $n = 32$ matched the minimum group size (12-month low-risk). The resulting high-risk-ASD-negative and low-risk control groups did not differ by age, sex, or scan site (see Tables 1 and 2). Mean ADOS severity scores (Gotham et al., 2009) did not differ significantly across age groups and only trended for significance across risk groups (see Table 3, where the multiple comparisons corrected critical $p = 0.025$).

2.3. Image acquisition

All scans were acquired at IBIS Network clinical sites using identical 3-T Siemens TIM Trio scanners (Siemens Medical Solutions, Malvern, PA) equipped with standard 12-channel head coils. Infants were naturally sleeping. The IBIS imaging protocol includes T1-weighted (T1W) and T2W anatomical imaging, 25-direction DTI and 65-direction HARDI DWI diffusion sequences, and resting state fcMRI (Wolff et al., 2012). This study made use of the 3-D sagittal T2W sequence (TE = 497 ms, TR = 3200 ms, matrix 256 × 256 × 160, 1 mm^3 voxels). Functional images were collected as a gradient-echo echo planar image (EPI) (TE = 27 ms, TR = 2500 ms, voxel size 4 mm × 4 mm × 4 mm, flip angle 90°, field of view 256 mm, matrix 64 × 64, bandwidth 1906 Hz). All presently analyzed infants (except two, see below) provided at least two fMRI runs, each run comprising 130 temporally contiguous frames (5.4 min).

2.4. fMRI preprocessing

Initial fMRI data preprocessing followed previously described procedures (Smyser et al., 2010). Briefly, these procedures included (i) compensation for slice dependent time shifts using sinc interpolation, (ii) correction of systematic odd-even slice intensity differences caused by interleaved acquisition, and (iii) spatial realignment to compensate for head motion within and across fMRI runs. The fMRI data were intensity scaled (one multiplicative constant over all voxels and frames) to obtain a whole brain mode value of 1000 (Ojemann et al., 1997). Such scaling facilitates the computation of variance measures

Table 2
Breakdown by sex and site.

	6 months	12 months	Total	Chi-square	Asymp. sig.
Sex					
Male	43	39	82		
Female	21	25	46		
Total	64	64	128	0.54	0.46
Scan location					
PHI	8	8	16		
SEA	8	11	19		
STL	35	33	68		
UNC	13	12	25		
Total	64	64	128	0.57	0.90

[2] Two 6-month infants and four 12-month infants exceeded the ASD threshold on the ADOS but did not meet diagnostic criteria according to DSM-IV-TR checklist at 24 months and were included in the current study.

Table 3
ADOS severity score at 24 months by age and risk.

Risk	Age	ADOS severity score		*df*	*t*	*p*
		Mean	SD			
High risk	6 months	1.6	0.9	62	−0.51	0.58
	12 months	1.7	1.7			
Low risk	6 months	1.3	0.7	62	−0.32	0.58
	12 months	1.4	0.9			
Age	Risk	ADOS severity score		*df*	*t*	*p*
		Mean	SD			
6 months	High risk	1.6	0.9	62	1.36	0.030
	Low risk	1.3	0.7			
12 months	High risk	1.7	1.0	62	1.45	0.075
	Low risk	1.4	0.9			

for purposes of quality assessment but does not alter computed correlations.

Atlas registration of the functional data was achieved by a sequence of affine transforms (fMRI average volume → T2W → atlas-representative target). In the present primary analyses, age specific (6 and 12 month) atlas-representative targets (Fonov et al., 2011) were used to account for shape differences across developmental age categories. Additional, control analyses, performed to exclude age-dependent biases, used a combined 6 + 12 month target generated as previously described (Buckner et al., 2004). The T2W was registered to the atlas representative template by 12-parameter affine transformation, optimizing a conventional spatial correlation, measure "NCC" (Pearson product-moment cross-correlation) in Holden et al. (2000). Subjects in which the optimized T2W → atlas voxel similarity measure fell below the 4th percentile were excluded from further analysis. Similarly, subjects with unreliable fMRI → T2W registration ($\eta < 0.35$; Rowland et al., 2005) were excluded from further analysis. Following fMRI → T2W → atlas transform composition, the volumetric time series were resampled in atlas space (3 mm^3 voxels) including correction for head movement in a single resampling step. Each atlas-transformed functional dataset was visually inspected in sagittal, transverse, and coronal views to exclude potential errors not otherwise identified.

2.5. Definition of regions of "non-interest" in atlas space

Owing to the tissue contrast properties at younger ages, automatic segmentation of infant structural images is extremely challenging (Hazlett et al., 2012). Therefore, white matter and CSF regions were manually defined in atlas-transformed T1-weighted images representing 15 subjects in each age group. These regions were eroded using a 2.5 mm Gaussian blurring kernel to reduce the risk of encroaching on gray matter. The intersection over each age group was computed to create white matter and cerebrospinal fluid (lateral ventricle) regions. These regions were used to extract nuisance regressors during fcMRI preprocessing (see Section 2.7).

2.6. Frame censoring

Head motion, even of sub-millimeter magnitude, has been identified as a non-physiological source of spurious variance in resting-state fMRI data (Power et al., 2012; Satterthwaite et al., 2013; Van Dijk et al., 2012). The present data therefore were subjected to frame censoring based on the frame-to-frame displacement (FD) measure (Power et al., 2014). The FD measure is calculated from the realignment parameters by converting rotational estimates to displacements on a sphere of 50 mm radius, and then differentiating the 6 motion estimates (*X*, *Y*, *Z*, pitch, yaw, roll) and summing their absolute values. Frames with FD > 0.2 mm were marked for censoring. Temporally isolated (fewer than 5 contiguous) FD < 0.2 mm frames were also censored. fMRI runs with fewer than 30 uncensored frames were discarded. To control for potential biases attributable to the amount of data per cohort, the first 150 non-censored (retained) fMRI frames were used for correlation analysis in each subject. All subjects had 110 frames censored, except two in the 12-month low-risk group: one with 107 frames censored out of 257 acquired (yielding 150 used frames), and one with 51 frames censored out of 201 acquired (yielding 150 used frames). Pre- and post-scrubbing mean frame displacement values are reported in Supplementary Table 4.

Supplementary Table 4 related to this article can be found, in the online version, at http://dx.doi.org/10.1016/j.dcn.2015.01.003.

2.7. fcMRI preprocessing

Further preprocessing in preparation for computation of ROI timeseries correlations followed procedures detailed in Power et al. (2014). The data were voxelwise demeaned and detrended within runs, ignoring censored frames. Nuisance waveforms then were voxelwise regressed from the data, ignoring censored frames. Nuisance regressors included (i) three translation (*X*, *Y*, *Z*) and three rotation (Pitch, Yaw, Roll) timeseries derived by retrospective head motion correction, together with expansion terms (24 total motion regressors) (Friston et al., 1996), and (ii) time series derived

from regions of non-interest (whole brain, white matter, and cerebrospinal fluid) and their 1st derivatives. Following nuisance regression, data in frames marked for censoring were replaced by interpolated values computed by least-squares spectral analysis (Mathias et al., 2004; Power et al., 2014). Please see Supplementary Tables 5 and 6 for information about the number of frames over which interpolation was implemented. Interpolated data were not included in the generation of correlation values, only for bandpass filtering. The fMRI data then were temporally filtered to retain frequencies in the $0.009\,Hz < f < 0.08\,Hz$ band. As a last step, the data were spatially smoothed using a Gaussian kernel (6 mm FWHM in each direction).

Supplementary Tables 5 and 6 related to this article can be found, in the online version, at http://dx.doi.org/10.1016/j.dcn.2015.01.003.

2.8. Definition of ROIs and correlation computation

Regions of interest (ROIs: $n = 280$) were defined from a combination of meta-analyses of autism studies (Philip et al., 2012) and of task data and cortical functional areal parcellations (Cohen et al., 2008) obtained in typical subjects (see Power et al., 2011). Three viewers (including authors SK and SH) inspected seed placements in age-specific atlas templates. 50 ROIs were partially outside the whole brain mask or showed differences in gray matter coverage at different ages. These ROIs were removed leaving 230 usable ROIs (218 from Power et al., 2011, 12 from Philip et al., 2012). Pairwise Pearson correlation values were generated from the average timecourse of voxels wholly contained by each 10 mm diameter spherical seed ROI. ROI sphere centers are reported (see Supplementary Table 1) in MNI152 space.

Supplementary Table 1 related to this article can be found, in the online version, at http://dx.doi.org/10.1016/j.dcn.2015.01.003.

2.9. Support vector machine (SVM) classification

Support vector machine (SVM) methods (Ben-Hur et al., 2008; Smola and Schölkopf, 2004) involved recent adaptations of those used by some of the authors (Dosenbach et al., 2010). SVM steps included *t*-test filtering to 200 features, linear kernel, soft margin separation, and leave-one-out-cross-validation (LOOCV; see Kohavi, 1995) (within group). SVM-related computations were carried out using the Spider Matlab Machine Learning Toolbox (http://www.kyb.tuebingen.mpg.de/de/bs/people/spider) implemented in MATLAB 7.8.0 (R2009a; The Mathworks, Natick, MA), as well as with functions available as part of the MATLAB Bioinformatics, Curve-fitting, and Statistics Toolboxes, and in-house MATLAB code.

Each (Fisher *z*-transformed) pairwise correlation was defined as a feature for use by the classifier. 26,335 two-sided (not assuming equal variance) *t*-tests were performed in each LOOCV fold. Within each fold, features were ranked by absolute *t*-score in descending order (the subject tested by the trained machine was also left out of the *t*-test filtering for that LOOCV fold), with the top 200 retained for classification (as in Dosenbach et al., 2010). Since every fold is unique, different feature combinations are possible. Features that were retained across folds were labeled as "consensus" features; e.g., those contained in 75% and 100% of the folds (75% and 100% consensus features) were used to construct our visualizations using CARET 5.65 (Van Essen et al., 2001).

2.10. Cross-site quality control of fMRI data

Multi-site studies may be affected by site-dependent differences in fMRI data quality (see, e.g., Tomasi and Volkow, 2011). To assess this question, the voxelwise temporal standard deviation over retained frames was averaged over the whole brain and plotted against mean FD (defined above) for each dataset (Supplementary Fig. 1). Inspection of these results revealed no evidence of clustering/separation of the data by site.

Supplementary Fig. 1 related to this article can be found, in the online version, at http://dx.doi.org/10.1016/j.dcn.2015.01.003.

2.11. Reporting of results

We report classifier accuracies, sensitivities, specificities, and *p*-values for binomial probabilities. For within-age analyses, sensitivity is defined as the percent of correctly classified as high-risk within all truly high-risk infants, and specificity as the percent of correctly classified participants as low-risk within all low-risk infants. For within-risk analyses, sensitivity is defined as the percent of correctly classified 12-month-olds within all truly 12-month-old infants, and specificity as the percent of correctly classified participants as 6-month-olds within all 6-month-old infants. *Training the SVMs within different groups also allowed us to test the classifiers' generalizations to data not trained on.* For example, LOOCV training for age classification on the low-risk data generates 64 SVMs (one for each LOOCV fold for the $n = 64$ datasets). Each high-risk dataset can then be tested on each of the low-risk-trained SVMs, and age classification accuracy would then be the average of these tests.

3. Results

3.1. SVM classifies age

The low- and high-risk groups provided independent samples for testing the classification of age based on fcMRI matrices, alone. SVMs classified 6- versus 12-month-old infants: low-risk – accuracy = 81.3%, sensitivity = 78.1%, specificity = 84.4%, $p = 5.03e\text{-}08$; and high-risk – accuracy = 75%, sensitivity = 81.3%, specificity = 68.8%, $p = 1.22e\text{-}05$. Control tests accounted for a number of possible alternative interpretations (see Section 3.3). The high- and low-risk-trained age-classifying SVMs only shared four common 100% consensus features and eight common 75% consensus features. Fig. 1 illustrates the eight shared 75% consensus features (Supplementary Table 2) and their involved regions/nodes for age classification of the high-risk and low-risk data. The visualizations

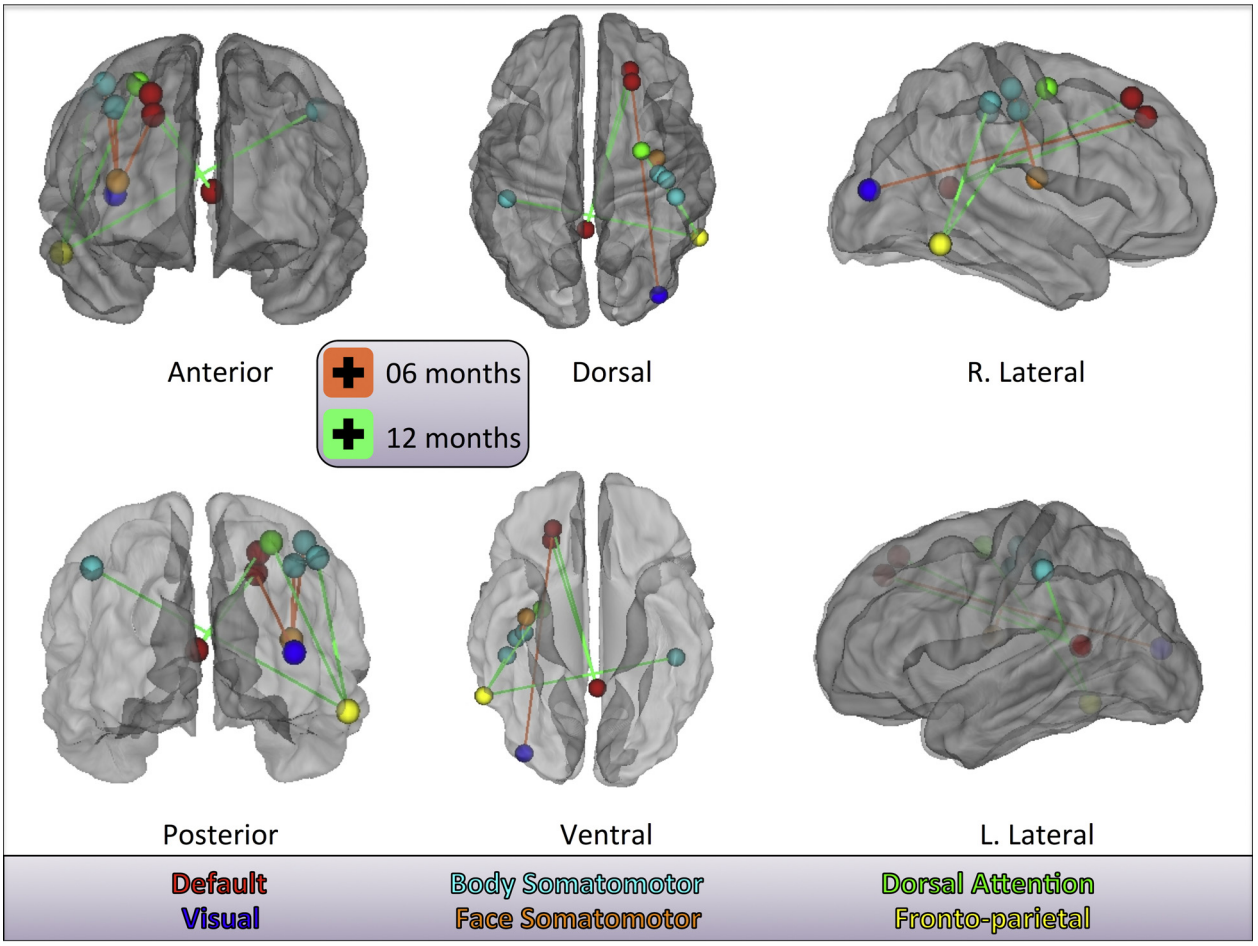

Fig. 1. 75% consensus features shared across risk group-specific SVMs. Lines represent features: green for functional connections that, when stronger, contribute to a classification of 12 months – and orange for functional connections that, when stronger, contribute to a classification of 6 months. Only 75% consensus (across cross-validation folds) features which are common to both the low- and high-risk-trained age-classifying SVMs are shown. Spheres represent involved nodes/seed regions. Node colors are the same as are assigned to adult networks in Power et al. (2011).

show contributions to accurate classification from functional connections between regions of interest (ROIs) which *in adults* would populate default mode, visual, body and face somatomotor, dorsal attention, and fronto-parietal networks. To assess further the importance of these eight shared 75% consensus features, we ran SVM for age classification in each risk group with only the subjects' eight corresponding functional connections. Classification accuracy was still high: low-risk – accuracy = 78.1%, sensitivity = 75%, specificity = 81.3%, $p = 9.40e\text{-}07$; and high-risk – accuracy = 87.5%, sensitivity = 93.8%, specificity = 81.3%, $p = 3.82e\text{-}11$. To explore potential degradation in SVM performance upon elimination of these eight features, we ran SVM for age classification in each risk group with the subjects' eight corresponding functional connections eliminated from potential entry into the *t*-test filtering step (200 features retained). Performance remained comparable: low-risk – accuracy = 79.7%, sensitivity = 78.1%, specificity = 81.3%, $p = 2.28e\text{-}07$; and high-risk – accuracy = 76.6%, sensitivity = 81.3%, specificity = 71.9%, $p = 3.53e\text{-}06$.

Supplementary Table 2 related to this article can be found, in the online version, at http://dx.doi.org/10.1016/j.dcn.2015.01.003.

3.2. Cross-group generalization and combined group analyses

SVMs could not classify *familial risk* for ASD at either age (again, all infants are ASD-negative): 6-month – accuracy for risk = 56.3%, sensitivity = 50%, specificity = 62.5%, $p = 0.130$; and 12-month – accuracy for risk = 57.8%, sensitivity = 53.1%, specificity = 62.5%, $p = 0.084$. Therefore, to test generalization of the age classification, we tested data from the high-risk infants with the low-risk-group-trained SVMs (i.e., with data they never trained on) and vice versa. As each classifier used a LOOCV method, there were a total of 64 SVMs for each risk group. Applying the high-risk-group-trained age-classifying SVMs to data from the low-risk infants resulted in an average accuracy of $88.2 \pm 3.52\%$ (mean ± SEM) (range 0–100%). The low-risk-group-trained age classifiers applied to the data

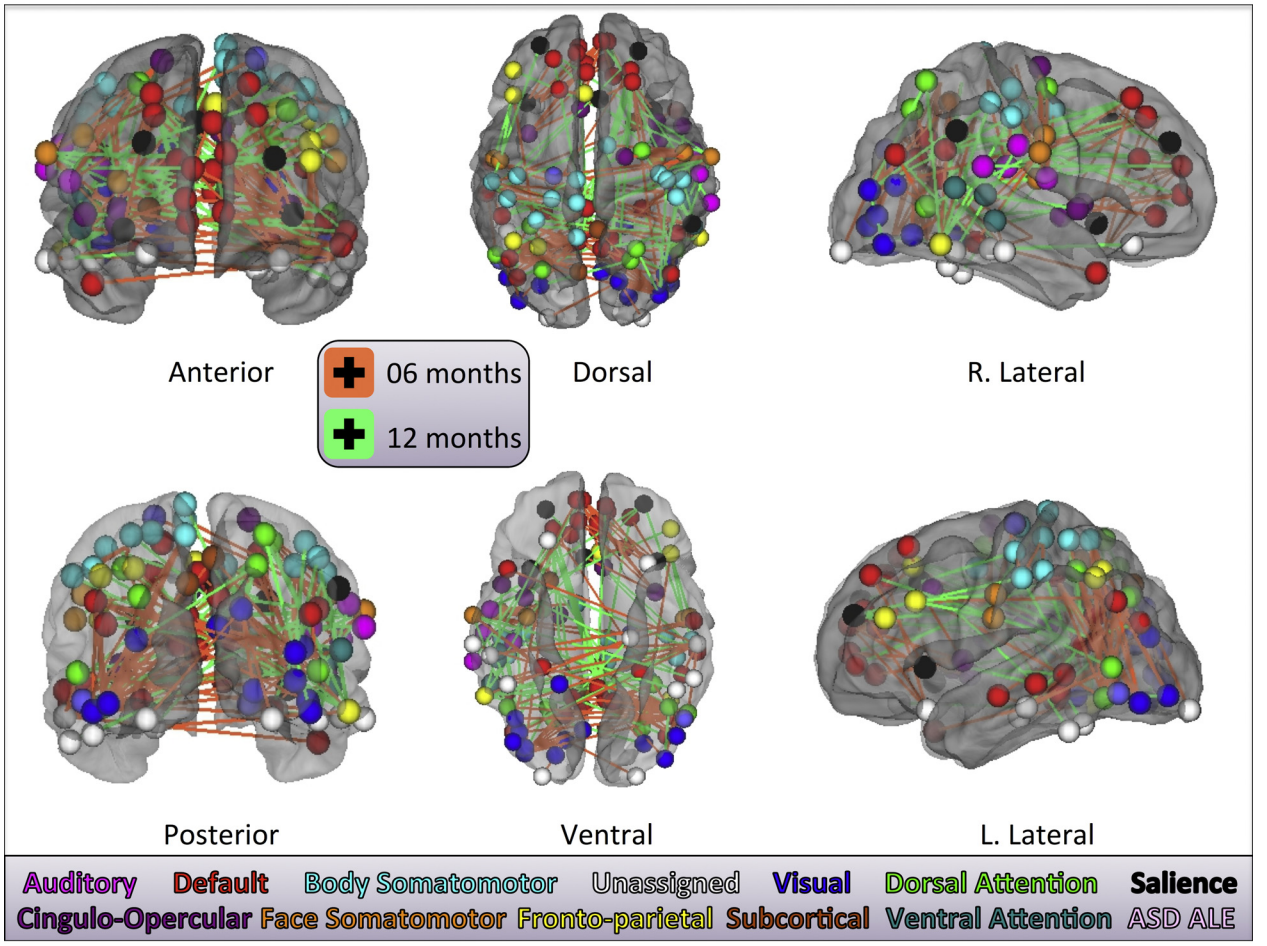

Fig. 2. The classification vector from the $n = 128$ run. Format is the same as in Fig. 1. Here, only 100% consensus (across all cross-validation folds) features are shown. Node colors are the same as are assigned to adult networks in Power et al. (2011); ASD ALE nodes are from Philip et al. (2012).

from the high-risk infants gave a similar accuracy of $85.2 \pm 3.67\%$ (range 0–100%).

Because SVM was unable to classify risk at each age, groups were then collapsed across risk, resulting in two larger groups for classifying age ($n = 128$ total datasets; $n = 64$ datasets/group). Here, SVM classification of 6- versus 12-month-olds was = 89.8% accurate, sensitivity = 92.2%, specificity = 87.5%, $p < 2.2251e\text{-}308$. The 100% consensus features for the classification vector for this run is visualized in Fig. 2 (see also Supplementary Table 3), which illustrates contributions to classification accuracy from 146 functional connections between ROIs which *in adults* would populate 12 of the 14 networks from Power et al. (2011) and also two ROIs taken from an ASD functional imaging activation likelihood estimation meta-analysis (Philip et al., 2012). The mean Euclidean distance for 12-month-contributing features (green lines) is 72.8 ± 4.0 mm in stereotaxic space, and that for the 6-month-contributing features (orange lines) is 65.9 ± 3.2 mm [$t(122.260^{3}) = -1.331$; $p = 0.186$].

Supplementary Table 3 related to this article can be found, in the online version, at http://dx.doi.org/10.1016/j.dcn.2015.01.003.

Finally, to test the stability of the eight shared 75% consensus features reported in Section 3.1, we also performed a 1000 iteration, leave-64-out-cross-validation procedure (that did not regard high-risk and low-risk groupings) using the $n = 128$ dataset. In this analysis, five of the eight shared 75% consensus features, for age classification across risk groups, were present 75% or more of the time, plus one new feature (these six features, and percent of iterations retained for all nine, are indicated in Supplementary Table 2).

3.3. Control analyses

3.3.1. Cross-sectional versus longitudinal data

To account for potential effects on SVM accuracy resulting from our mixed cross-sectional and longitudinal data, we created two completely cross-sectional groups of 6- and 12-month subjects (pooling across risk) and reran our analysis using the same parameters previously used for all other comparisons. In this analysis ($n = 44$/group: largest n

[3] Adjustment for unequal variances.

allowing a balanced SVM run with no subjects represented at both ages), SVM classification of 6 versus 12 months was 87.5% accurate, sensitivity = 86.4%, specificity = 88.6%, $p = 1.665e\text{-}14$.

3.3.2. Age-specific versus combined atlas-representative templates

To determine if the classification of age was influenced by registration to age-specific target representative atlas templates, SVM analyses were repeated using the same data registered to a single, cross-age atlas (see Section 2.4). SVM categorization was similar to that for the target-age atlas processed data. SVMs classified 6- versus 12-month-old infants: ($n = 32$ datasets/group) low-risk – accuracy = 89.1%, sensitivity = 87.5%, specificity = 90.6%, $p = 4.51e\text{-}12$; high-risk – accuracy = 84.4%, sensitivity = 87.5%, specificity 81.3%, $p = 1.77e\text{-}09$. For cross-age atlas processed data, SVM could not distinguish risk within age (6-month accuracy 43.8%, $p = 0.809$; 12-month accuracy 59.4%, $p = 0.052$). As above (Section 3.2), because SVM was unable to classify risk, we combined high and low risk together. For SVM on that data (classifying age) ($n = 128$), accuracy = 88.3%, sensitivity = 87.5%, specificity = 89.1%, $p < 2.2251e\text{-}308$.

3.3.3. Age-dependent differences in volume of gray matter contained in seed ROIs

All present fcMRI analyses were conducted on atlas-transformed data. Therefore, each ROI encompassed less absolute volume in the younger cohort. To account for potential effects of differential stretch into atlas space across age, we conducted another analysis that controlled for ROI sphere size and blurring kernel size effects on the 6- and 12-month data. For this analysis, we shrank the 12 month ROIs and blurring kernel by the inverse of the 6-month stretch factor to equate ROI size (for 12 month data 10 mm diameter is now 8.33 mm) and blur (6 mm is now 5 mm FWHM isotropic blurring kernel) in cohort native space. SVM ($n = 128$ datasets) still classified 6- versus 12-month-old infants with accuracy = 94.5%, sensitivity = 93.8%, specificity = 95.3%, $p < 2.2251e\text{-}308$.

4. Discussion

The second half of the first year of life is a time of radical motor, cognitive, linguistic, and social development (Csibra et al., 2000; Kouider et al., 2013; Kuhl et al., 2003; Pascalis et al., 2002; Tomasello, 2000) and a potentially critical time in the development of ASD (Zwaigenbaum et al., 2013). Our primary finding is that, after rigorous motion cleaning of the fcMRI data from this unique sample of infants, there is information sufficient to categorize subject age across this special period in infant development. Given recent concerns about fcMRI motion artifact effects (Power et al., 2012, 2014; Satterthwaite et al., 2013; Van Dijk et al., 2012), our results provide a critical extension of prior infant fcMRI findings (e.g., Damaraju et al., 2013; Gao et al., 2013, and see Hoff et al., 2013 for review). Here, data have been processed according to most recent frame-censoring, motion artifact rejection procedures (Power et al., 2014). The non-ASD low- and high-risk groups allowed us to explore generalization of our age classification results.

Interrogation of the most different correlations used for SVM provides two differing interpretations about the functional connections important for 6–12 month age classification. One might argue that only the functional connections supporting age classification which are common across separate samples (our risk groups) are truly important (i.e., the small number of connections that are strongly and consistently related to age classification). Alternatively, it may be argued that the power of SVM rests in its ability to leverage widely distributed but potentially less robust information (e.g., a much larger number of connections that are, individually, only weakly associated with age classification). These two considerations prompted us to explore: (a) SVM consensus features which are common across the age classifiers trained on the low- versus high-risk infant fcMRI matrices, and (b) consensus features from LOOCV training for age classification for the 128 datasets combined across risk. There were (only) eight common 75% consensus features for age classifiers trained in the different risk groups. Our leave-half-out-cross-validation run on the $n = 128$ dataset generally validated the stability of these eight features, as five of eight – plus one new feature – survived in 75% or more of the iterations (and the three that did not survive were present in 62%, 71%, and 72% of the iterations). These eight features may be particularly important because they are present in most of the LOOCV folds for SVMs trained on age with both high-risk and with low-risk data (effectively, a single iteration of a leave-half-out-cross-validation based on diagnostic grouping). These eight functional connections, alone, drove comparably accurate SVM classifications of age within each risk group. However, SVM performance did not degrade measurably with removal of these connections. When pooling across risk groups, the 100% consensus features for the 128 dataset analysis include 146 functional connections between ROIs which *in adults* would populate a majority of the networks from Power et al. (2011) plus ROIs from an ASD functional imaging meta-analysis (Philip et al., 2012). Thus, a small number of features may be sufficient for 6–12 month age classification in these infants, but there also remains widely distributed – spatially and in terms of the number of involved networks – information for age classification. The latter observation has face validity given the degree of motor, language, cognitive, and social developmental change over the 6–12 month time period. For example, involvement of somatomotor ROIs in our classifications may relate to developmental changes associated with the transition from crawling to walking. We chose to represent SVM consensus features in Figs. 1 and 2 without relative weighting to avoid potential over-interpretation of the biological significance of the extracted SVM weights (Haufe et al., 2014). The visualized features, however, were derived from consensus across *t*-test filtering, which *does* support their biological significance.

Other investigators have reported default mode network changes in infancy (Damaraju et al., 2013; Gao et al., 2009, 2013), and we note 29 involved default mode ROIs in our 100% consensus feature set (23 would be expected by chance, alone, based on 50 default mode

ROIs of the 230 used at input, and 108 represented in the 146 consensus features). Importantly, our work is unique in starting from functionally defined seeds, which we believe is critical for the proper interpretation of function network analysis results (Wig et al., 2011). The choice of such seeds enables demonstration of the additional importance of cingulo-opercular, dorsal attention, fronto-parietal, salience, body somatomotor, and visual networks, each of which are represented by more than 5 ROIs, for 6- versus 12-month age classification. Our demonstration of the involvement of default mode and dorsal attention network nodes in 6–12 month age classification (Supplementary Table 3) is important, given the recent report of strengthening default mode intra-network connectivity, and the development of anti-correlation between default mode and dorsal attention ROIs from birth to 12 months (see Gao et al., 2013). Though not exclusive, the 100% consensus features for the $n = 128$ dataset SVM run show a qualitative pattern whereby stronger functional connectivity for anterior–posterior functional connections contributes more to classification of 12 months, and that in posterior, left–right functional connections contribute more to classification of 6 months. These observations have superficial consistency with extant knowledge about patterns of white matter development in the first year of life. Investigators have described a sequence of myelination beginning in the cerebellum, pons, and internal capsule and advancing cranially to the optic radiations and splenium of the corpus callosum by approximately five months, following about a month later in the occipital and parietal lobes, and involving the frontal and temporal lobes and the genu of the corpus callosum after approximately eight months (e.g., Deoni et al., 2011). Elison and colleagues recently reported unique associations between visual orienting latencies and the microstructure of the splenium of the corpus callosum in 7-month-old low-risk infants (Elison et al., 2013b), and a correlation between fractional anisotropy in the right uncinate fasciculus at 6 months and the infants' response to joint attention bids at 9 months (Elison et al., 2013a). Although patterns of anatomical and functional connectivity are not the same, they are related (Damoiseaux and Greicius, 2009; Hagmann et al., 2008; Honey et al., 2009). Our forthcoming work includes fcMRI-diffusion tensor imaging (DTI) comparisons, which may reveal functional correlates for the above, recently published IBIS Network DTI findings.

Accumulating evidence suggests the 6–12 month period is a time when some of the defining behaviors of ASD begin to unfold (Zwaigenbaum et al., 2013). Our ASD-negative samples (high- and low-risk) allowed us to attempt SVM classification of familial risk for ASD. *For the reasons outlined below, this exercise had the primary purpose of generating a negative contrasting result that sets an important lower-bound against which to reference our positive age results.* Our present failure to classify accurately familial risk for ASD in no way precludes the possibility of an ASD functional connectivity endophenotype. The high-risk-ASD-negative group is expected to be a highly heterogeneous sample (and it is being characterized elsewhere by our group), with many infants developing typically, some developing sub-threshold ASD symptoms (Ozonoff et al., 2014), and others showing language and motor delays (Landa et al., 2012). A future clinical objective for our ongoing studies is to attempt ASD-positive (having the diagnosis) versus low- and high-risk-ASD-negative classifications to learn more about potentially discriminative features and to aid early risk assessment. Our present success with age-classification provides encouragement. We would have great concern about predictively classifying ASD versus typical development based on fcMRI data were we not able to classify infants on the basis of age at 6 versus 12 months. We await larger numbers of ASD-positive subjects in our on-going longitudinal studies to increase our power and to allow for future analyses focusing on sub-groups within the high-risk-ASD-negative sample.

One limitation of the present work is that there were not enough females ($n = 21$ at 6 and $n = 25$ at 12 months) to attempt SVM classification of sex. We employed a current frame-censoring approach for fcMRI motion censoring, and we considered the potential effects of differing atlas-target intermediaries and age-related stretches into analysis space. Although we have done what we can to minimize potential spurious differences, it is still possible that remaining systematic registration or image contrast differences may contribute to 6–12 month age classification. All structural image registration was accomplished using affine methodology. One advantage of this approach is that transform composition and inversion both are algebraically straightforward. Non-linear transformation can achieve a more precise atlas registration but is computationally less stable. It should be kept in mind that the BOLD fMRI data were acquired at $4\,mm^3$ voxel resolution and that susceptibility inhomogeneity-related EPI distortions were not corrected. Accordingly, the atlas transformation imprecision attributable to affine methodology arguably is not the greatest source of error. The issue of affine versus non-linear registration would be scientifically important if we were claiming to have defined the limits of SVM-based age classification, but we are not. The methodology as a whole is adequate to support our claims. The potential effects of using functionally defined ROIs from older subjects are also difficult to evaluate, presently. We are working to adapt recent advances in functional areal parcellation (Cohen et al., 2008) for infant fcMRI to generate infant-derived functional ROIs for future analyses. Finally, the infants were naturally sleeping during fcMRI acquisitions. Without simultaneous EEG, we can only assume that potential differences in sleep state across age did not contribute to our results. However, the percent of total sleep spent in rapid eye movement (REM) sleep decreases with development, along with other changes in sleep architecture (Roffwarg et al., 1966). Future studies will address questions about sleep-related effects on infant fcMRI data. Ongoing acquisitions will increase our sample size so that we will be able to make ASD-positive versus ASD-negative comparisons.

In conclusion, we brought a multivariate pattern classification approach to network-based fcMRI data from a large and unique infant study sample, processed with current motion correction procedures. Our age classification results demonstrate significant change in the structure

of large-scale functional brain networks over a 6-month period of dramatic cognitive, motor, and social transformation in the first year of life – a period which we suspect has great importance for understanding typical and atypical social-developmental trajectories (Elison et al., 2013a). We built our fcMRI matrices from functionally defined nodes and explored the most different correlations used for SVM in two different ways in relationship to known adult network definitions. In our next analyses we will apply graph theory-based analytic approaches to characterize in more detail the structures and properties of these infant networks, which appear qualitatively different in structure from adult functional brain networks after similar post-processing procedures. Our results encourage further basic examinations of large-scale functional brain network development in infancy. This work also sets the stage for studies of fcMRI correlates for emerging ASD at 6–12 months in later born siblings of children with ASD.

Conflict of interest

Dr. Robert C. McKinstry receives travel, lodging, meals, honoraria, acting and modeling fees from Siemens Healthcare (however, they are not related to this project) and consulting fees from Guerbet LLC. Dr. Alan C. Evans is a founder and a member of the Board of Directors of Biospective Inc. All other authors report no conflicts of interest.

Acknowledgements

We thank Jeffrey Neil, Terrie Inder, and Chris Smyser for contribution of an infant brain atlas and comparison scan sequence. We thank Weili Lin for technical and administrative support. We thank James Harper and Siyang Yang for assistance with selection of the ROIs. We would also like to thank Britt Gott and Teddi Gray for help with manuscript preparation. This work was supported by: R01 MH093510 (Pruett), R01 HD055741 (Piven), P30 NS048056 (Snyder), K12 EY016336 (Pruett, completed), and the McDonnell Center for Systems Neuroscience.

Appendix A. Members of IBIS Network

The Infant Brain Imaging Study (IBIS) Network clinical sites are located at the University of North Carolina (J. Piven, IBIS Network primary investigator; H.C. Hazlett, C. Chappell); the University of Washington (S.R. Dager, A.M. Estes, D. Shaw); Washington University (K.N. Botteron, R.C. McKinstry, J. Constantino, J. Pruett); Children's Hospital of Philadelphia (R.T. Schultz, S.J. Paterson); and the University of Alberta (L. Zwaigenbaum). The data coordinating center is at the Montreal Neurological Institute (A.C. Evans, D.L. Collins, G.B. Pike, P. Kostopoulos, S. Das). The image processing core is at the University of Utah (G. Gerig) and the University of North Carolina (M. Styner). The statistical analysis core is at the University of North Carolina (H. Gu).

References

American Psychiatric Association, 2000. Diagnostic and Statistical Manual of Mental Disorders, fourth ed., text rev. American Psychiatric Association, Washington, DC.

Ben-Hur, A., Ong, C.S., Sonnenburg, S., Schölkopf, B., Rätsch, G., 2008. Support vector machines and kernels for computational biology. PLoS Comput. Biol. 4 (10), e1000173.

Buckner, R.L., Head, D., Parker, J., Fotenos, A.F., Marcus, D., Morris, J.C., Snyder, A.Z., 2004. A unified approach for morphometric and functional data analysis in young, old, and demented adults using automated atlas-based head size normalization: reliability and validation against manual measurement of total intracranial volume. Neuroimage 23 (2), 724–738.

Cohen, A.L., Fair, D.A., Dosenbach, N.U., Miezin, F.M., Dierker, D., Van Essen, D.C., Schlaggar, B.L., Petersen, S.E., 2008. Defining functional areas in individual human brains using resting functional connectivity MRI. Neuroimage 41, 45–57.

Csibra, G., Davis, G., Spratling, M.W., Johnson, M.H., 2000. Gamma oscillations and object processing in the infant brain. Science 290 (5496), 1582–1585.

Damaraju, E., Caprihan, A., Lowe, J.R., Allen, E.A., Calhoun, V.D., Phillips, J.P., 2013. Functional connectivity in the developing brain: a longitudinal study from 4 to 9 months of age. Neuroimage 84, 169–180.

Damoiseaux, J.S., Greicius, M.D., 2009. Greater than the sum of its parts: a review of studies combining structural connectivity and resting-state functional connectivity. Brain Struct. Funct. 213 (6), 525–533.

Deoni, S.C., Mercure, E., Blasi, A., Gasston, D., Thomson, A., Johnson, M., Williams, S.C., Murphy, D.G., 2011. Mapping infant brain myelination with magnetic resonance imaging. J. Neurosci. 31 (2), 784–791.

Doria, V., Beckmann, C.F., Arichi, T., Merchant, N., Groppo, M., Turkheimer, F.E., Counsell, S.J., Murgasova, M., Aljabar, P., Nunes, R.G., et al., 2010. Emergence of resting state networks in the preterm human brain. Proc. Natl. Acad. Sci. U.S.A. 107 (46), 20015–20020.

Dosenbach, N.U., Nardos, B., Cohen, A.L., Fair, D.A., Power, J.D., Church, J.A., Nelson, S.M., Wig, G.S., Vogel, A.C., Lessov-Schlaggar, C.N., et al., 2010. Prediction of individual brain maturity using fMRI. Science 329 (5997), 1358–1361.

Elison, J., Wolff, J., Heimer, J., Paterson, S., Gu, H., Hazlett, H., Styner, M., Gerig, G., Piven, J., IBIS Network, 2013a. Frontolimbic neural circuitry at 6 months predicts individual differences in joint attention at 9 months. Dev. Sci. 16 (2), 186–197.

Elison, J.T., Paterson, S.J., Wolff, J.J., Reznick, J.S., Sasson, N.J., Gu, H., Botteron, K.N., Dager, S.R., Estes, A.M., Evans, A.C., et al., 2013b. White matter microstructure and atypical visual orienting in 7 month-olds at risk for autism. Am. J. Psychiatry 170 (8), 899–908.

Fonov, V., Evans, A.C., Botteron, K., Almli, C.R., McKinstry, R.C., Collins, D.L., 2011. Unbiased average age-appropriate atlases for pediatric studies. Neuroimage 54 (1), 313–327.

Fransson, P., Aden, U., Blennow, M., Lagercrantz, H., 2011. The functional architecture of the infant brain as revealed by resting-state fMRI. Cereb. Cortex 21 (1), 145–154.

Fransson, P., Skiöld, B., Engström, M., Hallberg, B., Mosskin, M., Aden, U., Lagercrantz, H., Blennow, M., 2009. Spontaneous brain activity in the newborn brain during natural sleep – an fMRI study in infants born at full term. Pediatr. Res. 66 (3), 301–305.

Friston, K.J., Williams, S., Howard, R., Frackowiak, R.S., Turner, R., 1996. Movement-related effects in fMRI time-series. Magn. Reson. Med. 35, 346–355.

Gao, W., Alcauter, S., Elton, A., Hernandez-Castillo, C.R., Smith, J.K., Ramirez, J., Lin, W., 2014. Functional network development during the first year: relative sequence and socioeconomic correlations. Cereb. Cortex [Epub ahead of print].

Gao, W., Gilmore, J.H., Giovanello, K.S., Smith, J.K., Shen, D., Zhu, H., Lin, W., 2011. Temporal and spatial evolution of brain network topology during the first two years of life. PLoS ONE 6 (9), e25278.

Gao, W., Gilmore, J.H., Shen, D., Smith, J.K., Zhu, H., Lin, W., 2013. The synchronization within and interaction between the default and dorsal attention networks in early infancy. Cereb. Cortex 23 (3), 594–603.

Gao, W., Zhu, H., Giovanello, K.S., Smith, J.K., Shen, D., Gilmore, J.H., Lin, W., 2009. Evidence on the emergence of the brain's default network from 2-week-old to 2-year-old healthy pediatric subjects. Proc. Natl. Acad. Sci. U.S.A. 106 (16), 6790–6795.

Gotham, K., Pickles, A., Lord, C., 2009. Standardizing ADOS scores for a measure of severity in autism spectrum disorders. J. Autism Dev. Disord. 39 (5), 693–705.

Gotham, K., Risi, S., Pickles, A., Lord, C., 2007. The Autism Diagnostic Observation Schedule: revised algorithms for improved diagnostic validity. J. Autism Dev. Disord. 37 (4), 613–627.

Hagmann, P., Cammoun, L., Gigandet, X., Meuli, R., Honey, C.J., Wedeen, V.J., Sporns, O., 2008. Mapping the structural core of human cerebral cortex. PLoS Biol. 6 (7), e159.

Haufe, S., Meinecke, F., Gorgen, K., Dahne, S., Haynes, J.D., Blankertz, B., Biessmann, F., 2014. On the interpretation of weight vectors of linear models in multivariate neuroimaging. Neuroimage 87, 96–110.

Hazlett, H.C., Gu, H., McKinstry, R.C., Shaw, D.W.W., Botteron, K.N., Dager, S.R., Styner, M., Vachet, C., Gerig, G., Paterson, S.J., et al., 2012. Brain volume findings in six month old infants at high familial risk for autism. Am. J. Psychiatry 169 (6), 601–608.

Hoff, G.E., Van den Heuvel, M.P., Benders, M.J., Kersbergen, K.J., De Vries, L.S., 2013. On development of functional brain connectivity in the young brain. Front. Hum. Neurosci. 7, 650.

Holden, M., Hill, D.L., Denton, E.R., Jarosz, J.M., Cox, T.C., Rohlfing, T., Goodey, J., Hawkes, D.J., 2000. Voxel similarity measures for 3-D serial MR brain image registration. IEEE Trans. Med. Imaging 19 (2), 94–102.

Honey, C.J., Sporns, O., Cammoun, L., Gigandet, X., Thiran, J.P., Meuli, R., Hagmann, P., 2009. Predicting human resting-state functional connectivity from structural connectivity. Proc. Natl. Acad. Sci. U.S.A. 106 (6), 2035–2040.

Johnson, M.H., 2001. Functional brain development in humans. Nat. Rev. Neurosci. 2 (7), 475–483.

Kohavi, R., 1995, August. A Study of Cross-validation and Bootstrap for Accuracy Estimation and Model Selection. Morgan Kaufmann Publishers, Montreal, Canada, pp. 1137–1145.

Kouider, S., Stahlhut, C., Gelskov, S.V., Barbosa, L.S., Dutat, M., de Gardelle, V., Christophe, A., Dehaene, S., Dehaene-Lambertz, G., 2013. A neural marker of perceptual consciousness in infants. Science 340 (6130), 376–380.

Kuhl, P.K., Tsao, F.M., Liu, H.M., 2003. Foreign-language experience in infancy: effects of short-term exposure and social interaction on phonetic learning. Proc. Natl. Acad. Sci. U.S.A. 100 (15), 9096–9101.

Landa, R.J., Gross, A.L., Stuart, E.A., Bauman, M., 2012. Latent class analysis of early developmental trajectory in baby siblings of children with autism. J. Child Psychol. Psychiatry 53 (9), 986–996.

Lin, W., Zhu, Q., Gao, W., Chen, Y., Toh, C.H., Styner, M., Gerig, G., Smith, J.K., Biswal, B., Gilmore, J.H., 2008. Functional connectivity MR imaging reveals cortical functional connectivity in the developing brain. Am. J. Neuroradiol. 29 (10), 1883–1889.

Lord, C., Risi, S., Lambrecht, L., Cook Jr., E.H., Leventhal, B.L., DiLavore, P.C., Pickles, A., Rutter, M., 2000. The Autism Diagnostic Observation Schedule-generic: a standard measure of social and communication deficits associated with the spectrum of autism. J. Autism Dev. Disord. 30 (3), 205–223.

Mathias, A., Grond, F., Guardans, R., Seese, D., Canela, M., Diebner, H.H., 2004. Algorithms for spectral analysis of irregularly sampled time series. J. Stat. Softw. 11 (2), 1–27.

Ojemann, J.G., Akbudak, E., Snyder, A.Z., McKinstry, R.C., Raichle, M.E., Conturo, T.E., 1997. Anatomic localization and quantitative analysis of gradient refocused echo-planar fMRI susceptibility artifacts. Neuroimage 6 (3), 156–167.

Ozonoff, S., Young, G.S., Belding, A., 2014. The broader autism phenotype in infancy: when does it emerge? J. Am. Acad. Child Adolesc. Psychiatry, 53.

Pascalis, O., de Haan, M., Nelson, C.A., 2002. Is face processing species-specific during the first year of life? Science 296 (5571), 1321–1323.

Philip, R.C., Dauvermann, M.R., Whalley, H.C., Baynham, K., Lawrie, S.M., Stanfield, A.C., 2012. A systematic review and meta-analysis of the fMRI investigation of autism spectrum disorders. Neurosci. Biobehav. Rev. 36 (2), 901–942.

Power, J.D., Barnes, K.A., Snyder, A.Z., Schlaggar, B.L., Petersen, S.E., 2012. Spurious but systematic correlations in functional connectivity MRI networks arise from subject motion. Neuroimage 59 (3), 2142–2154.

Power, J.D., Cohen, A.L., Nelson, S.M., Wig, G.S., Barnes, K.A., Church, J.A., Vogel, A.C., Laumann, T.O., Miezin, F.M., Schlaggar, B.L., et al., 2011. Functional network organization of the human brain. Neuron 72 (4), 665–678.

Power, J.D., Mitra, A., Laumann, T.O., Snyder, A.Z., Schlaggar, B.L., Petersen, S.E., 2014. Methods to detect, characterize, and remove motion artifact in resting state fMRI. Neuroimage 84, 320–341.

Roffwarg, H.P., Muzio, J.N., Dement, W.C., 1966. Ontogenetic development of the human sleep–dream cycle. Science 152 (3722), 604–619.

Rowland, D.J., Garbow, J.R., Laforest, R., Snyder, A.Z., 2005. Registration of [18F]FDG microPET and small-animal MRI. Nucl. Med. Biol. 32 (6), 567–572.

Satterthwaite, T.D., Wolf, D.H., Ruparel, K., Erus, G., Elliott, M.A., Eickhoff, S.B., Gennatas, E.D., Jackson, C., Prabhakaran, K., Smith, A., et al., 2013. Heterogeneous impact of motion on fundamental patterns of developmental changes in functional connectivity during youth. Neuroimage 83, 45–57.

Scaife, M., Bruner, J.S., 1975. The capacity for joint visual attention in the infant. Nature 253 (5489), 265–266.

Smola, A., Schölkopf, B., 2004. A tutorial on support vector regression. Stat. Comput. 14 (3), 199–222.

Smyser, C.D., Inder, T.E., Shimony, J.S., Hill, J.E., Degnan, A.J., Snyder, A.Z., Neil, J.J., 2010. Longitudinal analysis of neural network development in preterm infants. Cereb. Cortex 20 (12), 2852–2862.

Tomasello, M., 2000. Culture and cognitive development. Curr. Dir. Psychol. Sci. 9 (2), 37–40.

Tomasi, D., Volkow, N.D., 2011. Functional connectivity hubs in the human brain. Neuroimage 57 (3), 908–917.

Van Dijk, K.R., Sabuncu, M.R., Buckner, R.L., 2012. The influence of head motion on intrinsic functional connectivity MRI. Neuroimage 59 (1), 431–438.

Van Essen, D.C., Dickson, J., Harwell, J., Hanlon, D., Anderson, C.H., Drury, H.A., 2001. An integrated software suite for surface-based analyses of cerebral cortex. J. Am. Med. Inform. Assoc. 41, 1359–1378, See also http://brainmap.wustl.edu/caret

Wig, G.S., Schlaggar, B.L., Petersen, S.E., 2011. Concepts and principles in the analysis of brain networks. Ann. N.Y. Acad. Sci. 1224 (1), 126–146 http://www.ncbi.nlm.nih.gov/pubmed/21486299

Wolff, J.J., Gu, H., Gerig, G., Elison, J.T., Styner, M., Gouttard, S., Botteron, K.N., Dager, S.R., Dawson, G., Estes, A.M., et al., 2012. Differences in white matter fiber tract development present from 6 to 24 months in infants with autism. Am. J. Psychiatry 169 (6), 589–600.

Yeo, B.T.T., Krienen, F.M., Sepulcre, J., Sabuncu, M.R., Lashkari, D., Hollinshead, M., Roffman, J.L., Smoller, J.W., Zöllei, L., Polimeni, J.R., et al., 2011. The organization of the human cerebral cortex estimated by intrinsic functional connectivity. J. Neurophysiol. 106 (3), 1125–1165.

Zwaigenbaum, L., Bryson, S., Garon, N., 2013. Early identification of autism spectrum disorders. Behav. Brain Res. 251, 133–146.